ACS APPLIED MATERIALS & INTERFACES

Research Article

www.acsami.org

Nickel-Based Thin Film on Multiwalled Carbon Nanotubes as an Efficient Bifunctional Electrocatalyst for Water Splitting

Xingxing Yu, Tianyi Hua, Xiang Liu, Zhiping Yan, Peng Xu, and Pingwu Du*

Department of Materials Science and Engineering, CAS Key Laboratory of Materials for Energy Conversion, University of Science and Technology of China, Hefei, China 230026

Supporting Information

ABSTRACT: Herein, we report electrodeposited nickel-based thin film (NiO_x) on multiwalled carbon nanotubes (MWCNTs) as a highly efficient bifunctional catalyst for both the oxygen evolution reaction (OER) and hydrogen evolution reaction (HER). Under reductive conditions (−1.2 V vs Ag/AgCl), the hydrogen evolution catalyst (H_2-NiO_x) was facilely deposited on MWCNTs. The resulting film demonstrates good catalytic activity for hydrogen production in a near-neutral aqueous solution at low overpotential. When switched to oxidative conditions (+1.1 V vs Ag/AgCl), the amorphous H_2-NiO_x film onto MWCNTs can be transformed into another amorphous material (O_2-NiO_x) to efficiently catalyze OER. The NiO_x-MWCNTs catalyst was further characterized by scanning electron microscopy (SEM), energy-dispersive X-ray analysis (EDX), and X-ray photoelectron spectroscopy (XPS). The results show that the content of oxygen in the O_2-NiO_x-MWCNTs film is higher than that in the H_2-NiO_x-MWCNTs film. The NiO_x-MWCNTs catalyst has good catalytic stability, and the film is reversible when the potentials are switched between the reductive conditions and oxidative conditions. The Faradaic efficiencies of hydrogen and oxygen production are >95%.

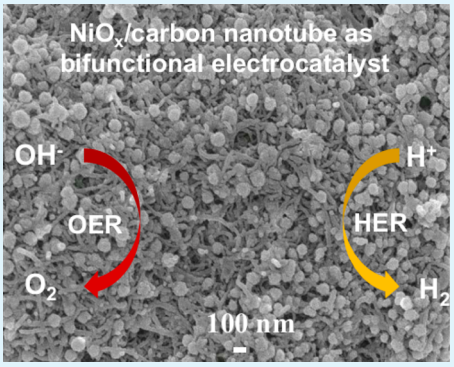

KEYWORDS: *electrocatalyst, oxygen evolution, hydrogen production, water splitting, nickel, bifunctional*

INTRODUCTION

Solar energy conversion has attracted much attention in recent decades. Efficient catalytic hydrogen evolution reaction (HER, $2H^+ + 2e^- \rightarrow H_2$) or oxygen evolution reaction (OER, $2H_2O \rightarrow O_2 + 4H^+ + 4e^-$) is a requirement for one-half of a solar water-splitting system.[1−3] Progress has been recently made in identifying catalysts capable of producing oxygen and hydrogen from water using either synthetic mimics of enzymes (hydrogenase and photosystem II (PS II) active site) or heterogeneous metal/metal oxide systems.[4−14] So far, the most efficient catalysts for HER and OER are still made from the precious metals (Pt for HER[15−17] and Ir or Ru for OER[11,18−20]), which may significantly hamper large-scale solar fuel production. The development of efficient water-splitting catalysts made of earth-abundant elements has therefore attracted much attention.[2,3,8] The typical abundant materials used for HER include MoS_2,[21−24] $NiMoN_x$,[25] Ni−Mo,[26] and Ni−Mo−Zn alloys.[14] In contrast, OER is considered to be more difficult because the water oxidation reaction involves a four-electron transfer process with the removal of four protons from water molecules.[27] In natural photosynthetic systems, the Mn_4CaO_5 cluster is used as the active site of photosystem II to oxidize water and release oxygen molecules. To closely imitate the catalytic functions of the Mn_4CaO_5 cluster, much effort has been devoted to the discovery of earth-abundant materials for water oxidation.[7,13,14,28] Recently, catalysts made of first-row transition metals for water oxidation have been widely explored, especially the catalysts made of cobalt, manganese, and nickel.[7,8,10,29−33] However, in terms of the catalytic efficiency and stability, water splitting remains a great challenge in the conversion of solar energy into chemical fuels.

More recently, a bifunctional cobalt-based material was reported to catalyze both hydrogen evolution and oxygen evolution by switching the applied electrochemical potential.[34] A similar result was also found in a nickel-based material.[35] On the basis of these findings, it is possible to simultaneously prepare HER and OER catalysts under the same conditions by a simple electrodeposition method. However, these bifunctional materials suffered from their low catalytic performance for both HER and OER. In this present study, we reported an approach to improve the catalytic activity of a nickel-based bifunctional material by electrodepositing it onto multiwalled carbon nanotubes (MWCNTs). MWCNT materials have been widely used to transfer and store energy due to their advantages of high surface area, high electrical conductivity, and structural flexibility.[30,36−38] The nickel-based bifuncational catalyst (NiO_x-MWCNTs) was facilely prepared by reduction-induced electrodeposition in a potassium borate buffered solution containing Ni^{2+} under near-neutral conditions. The catalyst can effectively catalyze both hydrogen evolution and oxygen evolution at low overpotentials with good stability. Under the

Received: June 19, 2014
Accepted: August 19, 2014
Published: August 19, 2014

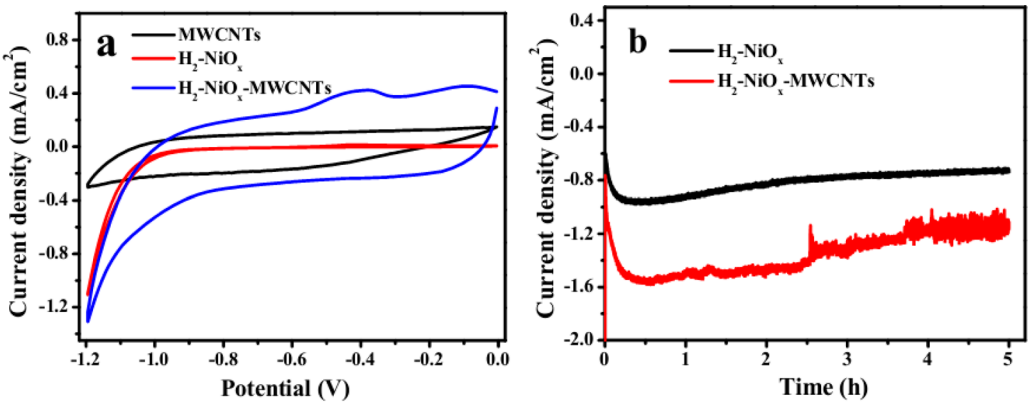

Figure 1. Electrochemical performance of the H_2-NiO_x-MWCNTs catalyst under reductive conditions for the hydrogen evolution reaction. (a) CV curves using ITO (red) and MWCNTs/ITO (blue) as the working electrodes in a 0.1 M KBi solution (pH 9.2) containing 0.1 mM Ni^{2+}. Black plot is the control experiment using the MWCNTs/ITO electrode in a 0.1 M KBi solution at pH 9.2 with no Ni^{2+}. The scan rate is 50 mV/s with *iR* compensation. (b) Current density profiles for bulk electrolysis using an ITO (black) and MWCNTs/ITO (red) electrode at −1.2 V in a 0.1 M KBi solution (pH 9.2) containing 0.1 mM Ni^{2+}.

same conditions, it is fully reversible to conduct the reductive process and oxidative process by altering the applied electrochemical potential.

EXPERIMENTAL SECTION

Materials. All chemical reagents, including nickel nitrate hexahydrate ($Ni(NO_3)_2{\cdot}6H_2O$), boric acid (H_3BO_3), potassium hydroxide (KOH), potassium borate (KBi), ethanol, *N*-methyl-2-pyrrolidone (NMP), and 5 wt % Nafion solution, are commercially available (Aldrich or Acros) and used without further purification. MWCNTs were purchased from Chengdu Organic Chemistry Co., Ltd., and indium tin oxide (ITO, 8−12 Ω /sq) glass was purchased from Zhuhai Kaivo Electronic Components Co., Ltd. The ITO glass plates were ultrasonicated in deionized water, ethanol, and deionized water for 3 min, successively, and dried in air.

Fabrication of MWCNTs/ITO Electrodes. The fabrication of MWCNTs/ITO electrodes was as follows: 5 mg of MWCNTs was dispersed in 1 mL of *N*-methyl-2-pyrrolidone (NMP), followed by the addition of 100 μL of 5% Nafion solution. The MWCNT suspension was homogenized by ultrasonic dispersion for 20 min to make MWCNT ink. Using a pipet, 30 μL of the resulting ink was carefully dropped onto clean ITO glass within an area of about 1 cm^2. The as-prepared MWCNTs/ITO electrodes were put into a vacuum oven at 100 °C for 3 h. The final MWCNTs/ITO electrodes were used as the working electrodes for electrochemical experiments.

Cyclic Voltammetry (CV). All of the following electrochemical experiments were performed at room temperature with a CHI602D Instrument Potentialstat (Shanghai Chen Hua Instrument Co., Ltd.). In a typical three-electrode system, MWCNTs/ITO or ITO glass plates were used as the working electrode, with an Ag/AgCl electrode (3 M KCl, with potential of 0.21 V vs NHE) as the reference electrode and platinum wire as a counter electrode. The electrolyte solution was 0.1 M potassium borate (KBi) solution at pH 9.2 containing 0.1 mM Ni^{2+} or no Ni^{2+}, and all the potentials reported in this article were versus an Ag/AgCl reference electrode. All of the cyclic voltammograms were measured at 50 mV/s with *iR* compensations and no stirring.

Bulk Electrolysis. The nickel-based catalyst was electrodeposited onto the MWCNT/ITO electrode surface at −1.2 V during bulk electrolysis in a 0.1 M KBi solution at pH 9.2 containing 0.1 mM Ni^{2+}. The nickel-based catalyst was also electrodeposited onto the ITO electrode under the same conditions to compare the catalytic activities for water splitting. The electrodeposited NiO_x-MWCNTs were then transferred to a 0.1 M KBi solution at pH 9.2 without Ni^{2+} to study the water oxidation reaction at an applied potential of +1.1 V.

Tafel Plot. The NiO_x-MWCNT catalyst was electrodeposited after 1 C of charges passed through the working electrode at −1.2 V in a 0.1 M KBi solution at pH 9.2 containing 0.1 mM Ni^{2+}. Then the NiO_x-MWCNT electrode was transferred to a 0.1 M KBi solution at pH 9.2 without Ni^{2+}. The Tafel plot was obtained by performing bulk electrolysis in the solution at variable applied potentials when the steady current was achieved. The applied potentials were varied from 0.65 to 0.80 V, and the intervals were 25 mV.

Hydrogen Generation Reaction. The catalytic hydrogen production experiments were performed in a gastight electrochemical cell. The solution of 0.1 M KBi at pH 9.2 containing 0.1 mM Ni^{2+} was degassed by bubbling with high purity N_2 for 20 min with vigorous stirring. Hydrogen gas evolution was measured by gas chromatography (SP-6890, nitrogen as a carrier gas) with thermal conductivity detection (TCD).

Faradaic Efficiency. A fluorescence-based oxygen sensor (Ocean Optics) was used for quantitative detection of O_2. The experiment was also performed in a gastight electrochemical cell. The solution of 0.1 M KBi without Ni^{2+} was degassed by bubbling with high purity N_2 for 20 min with vigorous stirring. The NiO_x-MWCNT electrode was used as the working electrode. The reference electrode was positioned several millimeters (2−4 mm) from the NiO_x-MWCNT electrode. O_2 content from the FOXY probe, recorded at 2 s intervals, was converted into the partial pressure of O_2 in the headspace. After calibration, bulk electrolysis was initiated at +1.1 V.

X-ray Diffraction (XRD). The phase analysis of the H_2-NiO_x-MWCNTs and O_2-NiO_x-MWCNTs catalyst materials was measured by X-ray diffraction (XRD, D/max-TTR III) via graphite monochromatized Cu Kα radiation of 1.5406 Å, operated at 40 kV and 200 mA. The scanning rate was 5° min^{-1} from 10° to 70° in 2θ.

Scanning Electron Microscopy (SEM) and Energy-Dispersive X-ray Analysis (EDX). SEM images and EDX spectra were obtained using a SIRION200 Schottky field emission scanning electron microscope (SFE-SEM) equipped with a Rontec EDX system. The detected samples were rinsed with deionized water and dried in air, then coated with Pt to make the samples conductive before loading into the instrument. Images were obtained with an acceleration voltage of 5 kV or 10 kV.

Transmission Electron Microscopy (TEM). The morphologies of the samples were further analyzed by TEM. TEM images were obtained on a JEM-2011 electron microscope, operated at an acceleration voltage of 200 K.

X-ray Photoelectron Spectroscopy (XPS). The elemental composition of the catalysts on the surface of the electrode and the valence states of metal elements were probed with an ESCALAB 250 X-ray photoelectron spectroscope (XPS). The survey scan and the high resolution Ni 2p spectra were obtained. The spectra are referenced to the C 1s peak (285.0 eV).

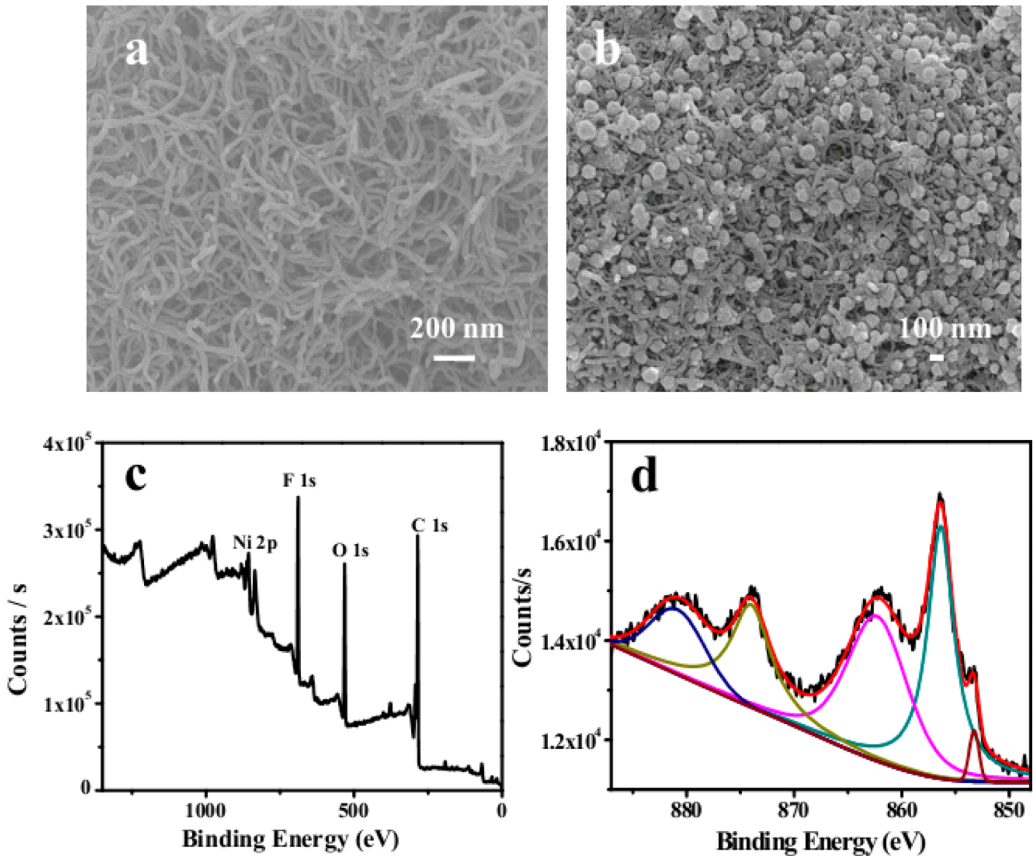

Figure 2. (a) SEM image of the MWCNTs. (b) The surface of the H_2-NiO_x-MWCNTs electrode after 8 h of electrodeposition at −1.2 V in a 0.1 M KBi solution containing 0.1 mM Ni^{2+}. (c) XPS survey of the H_2-NiO_x-MWCNTs electrocatalyst. (d) Ni 2p character.

RESULTS AND DISCUSSION

Figure 1a shows the cyclic voltammogram (CV) curves of ITO and MWCNT/ITO electrode in a 0.1 M KBi solution at pH 9.2 containing 0.1 mM Ni^{2+}. An Ag/AgCl electrode was used as the reference electrode and a Pt wire as the counter electrode. The scan range varied from 0 V to −1.2 V (all the potentials in this article are versus Ag/AgCl). The cathodic scan using ITO as the working electrode shows a sharp catalytic wave for HER with an onset potential at −0.98 V (Figure 1a, red plot). Interestingly, when a MWCNT/ITO was used as the working electrode, the onset catalytic potential was shifted to −0.83 V, which is ∼150 mV lower than the onset value using bare ITO as the working electrode. This observation indicates that the MWCNTs electrode can significantly lower the overpotential and highly enhance the catalytic performance of the NiO_x catalyst for hydrogen production from water. The produced hydrogen gas has been confirmed by gas chromatography (GC). In addition, in the control experiment performed in a 0.1 M nickel-free KBi solution, no appreciable catalysis for hydrogen production was observed on the MWCNT/ITO electrode at −1.2 V (Figure 1a, black plot). This result indicates that the existence of both MWCNTs and Ni^{2+} is crucial for catalytic hydrogen production under a low overpotential.

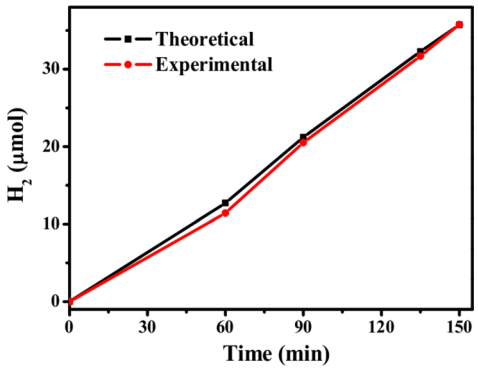

Figure 3. Hydrogen production during bulk electrolysis measured by gas chromatography (red dots) and the theoretical amount of hydrogen calculated by the passed charges through the H_2-NiO_x-MWCNT working electrode at −1.2 V in a 0.1 M KBi solution containing 0.1 mM Ni^{2+} (black dots).

The current density profiles for bulk electrolysis under reductive conditions using the ITO or MWCNT/ITO electrode are shown in Figure 1b. The experiments were run in a 0.1 M KBi buffered solution at pH 9.2 containing 0.1 mM Ni^{2+}, and the applied potential was −1.2 V. The electrodeposited material is named as H_2-NiO_x. A stable current density using a bare ITO electrode was achieved at 0.77 mA/cm^2. In contrast, the MWCNT/ITO electrode has an enhanced catalytic current density at 1.25 mA/cm^2, which is 62% higher than that of the bare ITO electrode under the same conditions. The results indicate that MWCNTs can greatly improve the catalytic performance of the HER, which is probably attributable to the MWCNTs facilitating the transport of electrons to the surface of the nickel-based catalyst in the process of hydrogen production. The stable current density has no significant decrease even after 36 h of electrolysis (Figure S1, Supporting Information), demonstrating that the H_2-NiO_x-

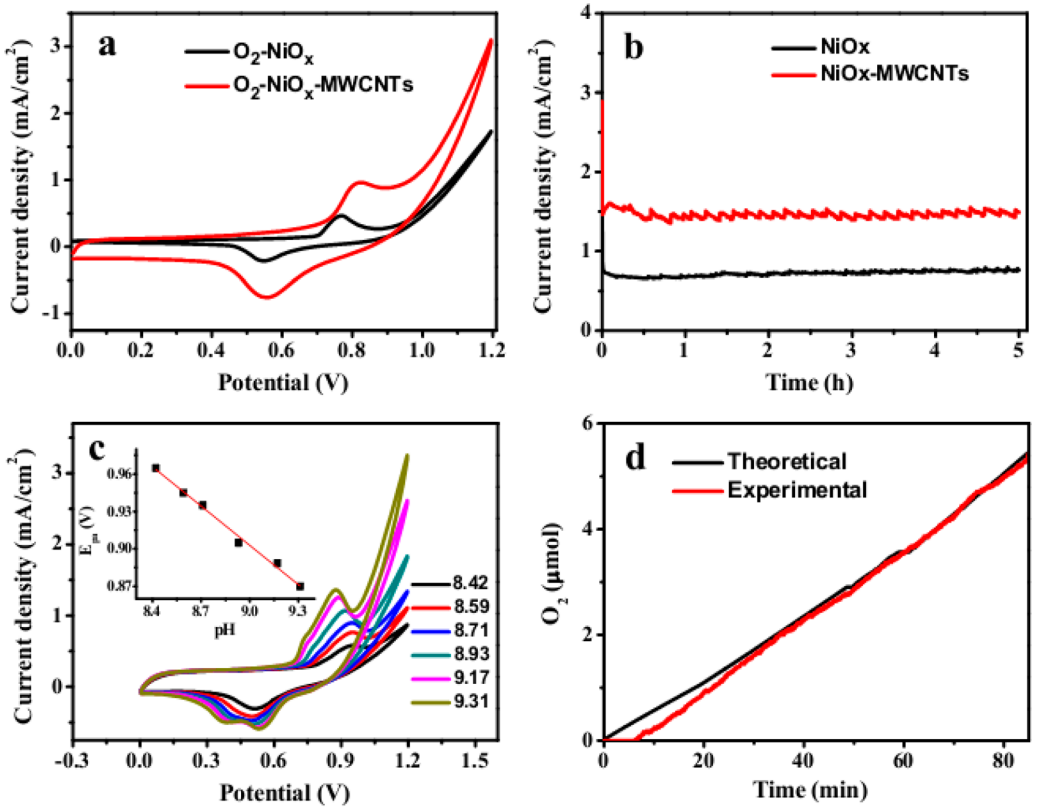

Figure 4. Electrochemical performance of O_2-NiO_x-MWCNTs and O_2-NiO_x catalysts in a 0.1 M KBi solution (pH 9.2) without Ni^{2+}. (a) CV curves of O_2-NiO_x-MWCNTs and O_2-NiO_x at the scan rate of 50 mV/s with *iR* compensation. (b) Current density profiles of O_2-NiO_x-MWCNTs and O_2-NiO_x for bulk electrolysis at +1.1 V. (c) CV curves of O_2-NiO_x-MWCNTs under various pH values from 8.42 to 9.31. The scan rate is 50 mV/s. The inset shows that the slope of the linear fit for E_{pa} to pH is −100 mV per pH unit. (d) O_2 production for the O_2-NiO_x-MWCNT catalyst, measured by a fluorescence-based oxygen sensor (red plot) and the theoretical amount of O_2 produced (black plot), at +1.1 V in a 0.1 M KBi solution (pH 9.2) without Ni^{2+}.

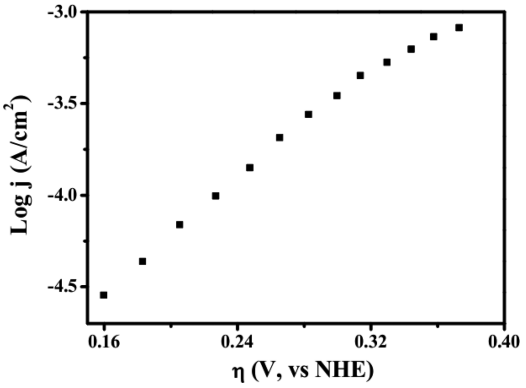

Figure 5. Tafel plot. The applied potential varied from 0.65 to 0.93 V (vs Ag/AgCl). $\eta = V_{appl} - iR - E_{pH}$, where V_{appl} is the applied potential vs NHE, and E_{pH} = 1.23 V − 0.059 pH.

MWCNTs electrocatalyst has good stability during bulk electrolysis.

The surface morphologies of MWCNTs and electrodeposited H_2-NiO_x-MWCNTs are shown in Figure 2a,b. The H_2-NiO_x-MWCNTs sample was obtained after 8 h of bulk electrolysis at −1.2 V in a 0.1 M KBi buffered solution (pH 9.2) containing 0.1 mM Ni^{2+}. SEM images show that the MWCNTs possess tubular structure. The structure of the H_2-NiO_x-MWCNTs sample in Figure 2b has a similar tubular shape, and the H_2-NiO_x particles were evenly dispersed on the surface of MWCNTs. The MWCNTs are the substrate to support the electrodeposited H_2-NiO_x nanomaterial, as shown in TEM images (Figure S2, Supporting Information). In contrast to the SEM image, the H_2-NiO_x nanoparticles on MWCNTs from the TEM image are not well dispersed probably because of the sonication before TEM measurement. The element composition of the electrodeposited H_2-NiO_x-MWCNTs was analyzed by energy-dispersive X-ray analysis (EDX), as shown in Figure S3 (Supporting Information). The EDX spectrum demonstrates that Ni, O, C, K, and Pt are the main elements on the surface of the electrodeposited H_2-NiO_x on MWCNTs. The Ni and O are the elements from the H_2-NiO_x catalyst, and the C can be attributed to MWCNTs on the ITO glass plate. The K is from the KBi electrolyte, and the Pt was artificially sprayed on the surface of the H_2-NiO_x-MWCNTs film to improve conductivity.

Furthermore, the electrodeposited H_2-NiO_x-MWCNTs catalyst was analyzed by XPS (Figure 2c). The XPS spectra show the presence of Ni, O, and C elements on the surface of the working electrode, which is consistent with the results obtained by EDX. The Ni and O should be from H_2-NiO_x nanomaterial, and the high resolution Ni 2p peaks are shown in Figure 2d. In Ni 2p spectra, two typical sets of broad signals were observed, corresponding to Ni $2p_{3/2}$ (856.28 eV) and Ni $2p_{1/2}$ (873.78 eV), indicating that the Ni element is in a range of typical Ni^{2+} or Ni^{3+} bound to oxygen.[32] The O 1s signal is located at 531.6 eV, and the major C 1s peak is located at 285.0 eV. The peak of C 1s could be from both MWCNTs and the reference C peak. The XPS data show that the element ratio of

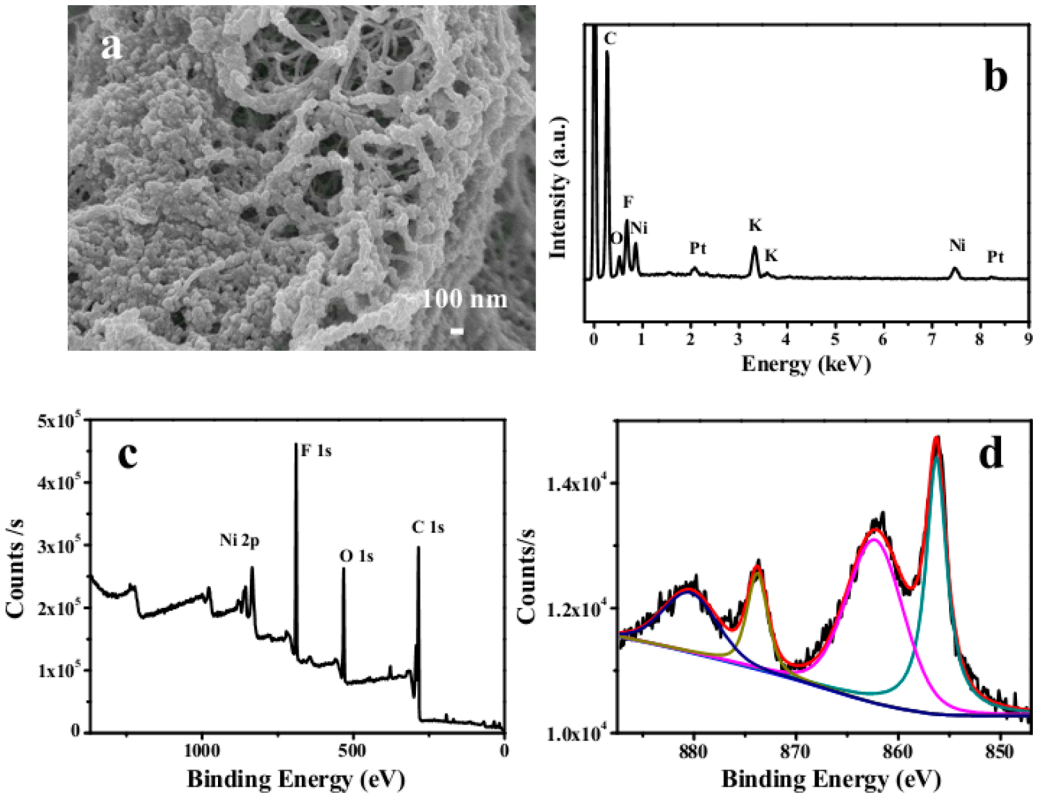

Figure 6. (a) SEM image of the O_2-NiO_x-MWCNT catalyst under an anodic potential for 8 h. (b) EDX pattern of the O_2-NiO_x-MWCNT catalyst. (c) XPS survey of the O_2-NiO_x-MWCNT catalyst. (d) Ni 2p character.

C, O, and Ni in the H_2-NiO_x-MWCNTs film is about 16.2:5.7:1.0 (56.93%, 20.01%, and 3.51%, for C, O, Ni, respectively). According to the previous studies, the $Ni(OH)_2$ peaks appeared at 856−857 eV with related satellite peaks due to shakeup processes at 860−865 eV (Ni 2p 3/2 region), and the O peak showed up at ∼532 eV (O 1s).[39,40] It is probably that the catalyst films mainly contain $Ni(OH)_2$. However, NiOOH also has quite similar XPS features as $Ni(OH)_2$ with broad peaks at 855−856 eV (Ni 2p3/2) and 532 eV (O 1s).[41,42] The appearance of a shoulder peak at around 854.13 eV might indicate the presence of another form of Ni species. The absence of the O peak at ∼529 eV may exclude the existence of NiO.[39,40]

A catalytic HER was performed in a gastight electrochemical cell under inert atmosphere. Bulk electrolysis was run at −1.2 V in a 0.1 M KBi solution (pH 9.2), and the amount of hydrogen gas was measured by GC. The hydrogen bubbles were rapidly produced on the MWCNTs/ITO electrode, and GC data showed the rise of hydrogen percentage in the headspace of the electrochemical cell. The theoretical amount of hydrogen was calculated by assuming that the total charge was from $2e^-$ reduction of protons by Faraday's law. The amount of produced hydrogen in the experiment matched well the theoretical amount of hydrogen under the total charge during the process of electrolysis over 150 min, corresponding to an efficiency of >98% (Figure 3).

The as-deposited H_2-NiO_x-MWCNTs electrocatalyst was further transferred to a nickel-free 0.1 M KBi solution at pH 9.2 to study the electrocatalytic OER activity. The anodic scan using the H_2-NiO_x-MWCNTs electrode exhibits a broad wave of nickel ion oxidation at $E_{p,a}$ = +0.76 V, followed by an obvious catalytic wave with an onset catalytic potential at +0.91 V (Figure 4a). Under this oxidative condition, the H_2-NiO_x catalyst is transformed into another amorphous form, which is named as O_2-NiO_x. Interestingly, the anodic scan shows a broad wave of nickel ion oxidation at $E_{p,a}$ = +0.82 V, but the current density of the sharp catalytic wave was much higher than that without MWCNTs. The presence of the enhanced catalytic wave prompted us to examine the electrode activity during bulk electrolysis. Current density profiles of O_2-NiO_x-MWCNTs and O_2-NiO_x at a fairly positive potential (+1.1 V versus Ag/AgCl) for bulk electrolysis are shown in Figure 4b. A stable current density of 1.5 mA/cm^2 was achieved for O_2-NiO_x-MWCNTs, which is much higher than that for O_2-NiO_x without MWCNTs (0.8 mA/cm^2). Both of the electrocatalysts have good stability for oxygen evolution during 5 h of bulk electrolysis (Figure 4b). The pH dependence of the electrodeposited O_2-NiO_x on MWCNTs was examined via the CV scans (Figure 4c). The redox potentials of O_2-NiO_x-MWCNTs are highly dependent on the pH values, indicating that a proton-coupled electron transfer process is involved in this system. The oxidation waves are gradually shifted to a lower potential under a higher pH, which reflects the shifts in the thermodynamic potential for water oxidation. CV experiments conducted at a scan rate of 50 mV/s give rise to a plot of $E_{p,a}$ vs pH with a slope of −100 mV per pH unit (Figure 4c, inset), which is different from the theoretical value of −59 mV per pH unit expected for a $1e^-$-$1H^+$ redox process from $Ni^{II}(OH)_2$ to $Ni^{III}O(OH)$. This result shows that the loss of $1e^-$ is probably accompanied by the transfer of ∼1.5 protons.[43−45]

The Faradaic efficiency of the O_2-NiO_x-MWCNTs electrocatalyst was measured by a fluorescence-based oxygen sensor (Figure 4d). Bulk electrolysis was performed at +1.1 V in a 0.1 M nickel-free KBi solution (pH 9.2) in a gastight electro-

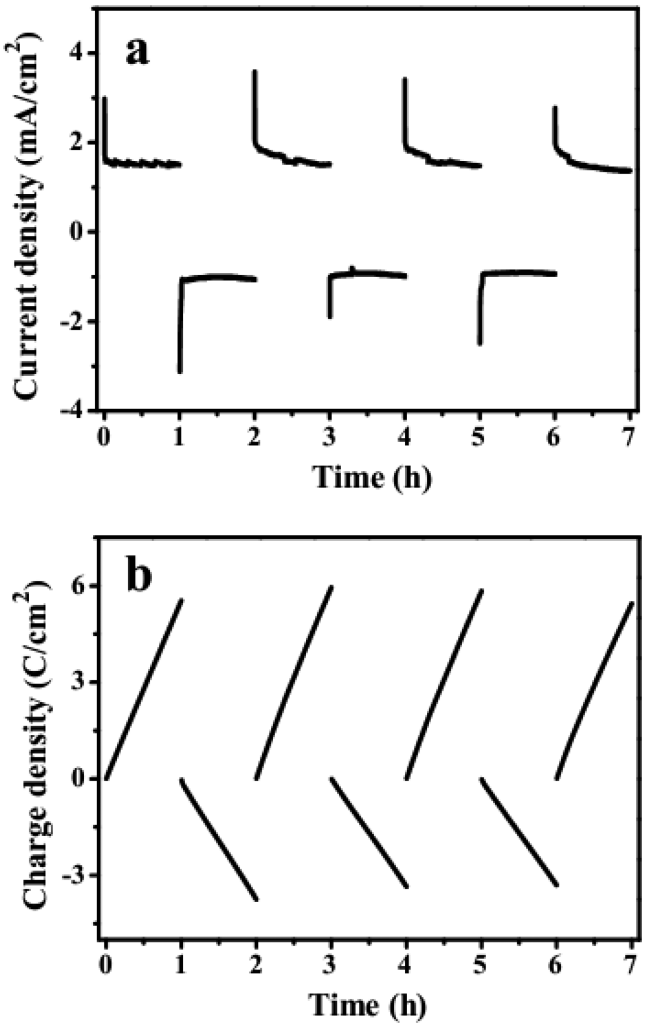

Figure 7. (a) Current density and (b) charge density as a function of time using NiO_x-MWCNT catalyst for water splitting. The NiO_x-MWCNT catalyst was prepared by electrodeposition at −1.2 V in a 0.1 M KBi solution (pH 9.2) containing 0.1 mM Ni^{2+}. The catalyst was then transferred to the same buffered solution without Ni^{2+}. Bulk electrolysis for oxygen evolution was performed at +1.1 V for 1 h, then the applied potential was switched to −1.2 V for hydrogen production.

chemical cell under nitrogen. The theoretical amount of oxygen evolution under the applied potential +1.1 V was calculated by assuming that the total charge was from $4e^-$ oxidation of water by Faraday's law. The amount of oxygen was a good match for the theoretical amount of oxygen under the total charge during the process of electrolysis, corresponding to a Faradaic efficiency of >95% in 85 min (Figure 4d), showing that the O_2-NiO_x-MWCNTs electrocatalyst is highly effective for water oxidation.

The Tafel plot was obtained by measuring the stable current density (j) of O_2-NiO_x-MWCNTs (obtained after 1 C of charges passed through the electrode at +1.1 V) at various potentials for water oxidation, as a function of the overpotential (η) (Figure 5). The slope of the Tafel plot ranging from 0.65 to 0.93 V is 137 mV per decade, which is outside the range of 40−80 mV per decade for typical Ni oxides.[44,46,47] A current density of 0.5 mA/cm^2 requires η = 0.33 V, which is much lower than the previous report using nickel-based catalysts for oxygen evolution, such as Ni−Bi film (0.5 mA/cm^2 requires η = 0.41 V).[44]

The surface morphologies of the O_2-NiO_x-MWCNTs catalyst were measured by SEM and TEM (Figure 6a and Figure S4, Supporting Information). The image shows nanotubes and O_2-NiO_x nanoparticles. The nanotubes are from the MWCNTs, and the O_2-NiO_x nanoparticles are uniformly dispersed on the nanotubes. The close contact of the MWCNTs and O_2-NiO_x indicates that MWCNTs can effectively enhance the transport of electrons during the OER. The element composition of the O_2-NiO_x-MWCNTs sample was measured by EDX (Figure 6b). The EDX spectrum demonstrates that Ni, O, C, K, and Pt are the main elements in the catalyst, which is similar to the result for the H_2-NiO_x-MWCNTs film electrodeposited at −1.2 V. Moreover, the element composition and element valence states of the O_2-NiO_x-MWCNTs were further analyzed by XPS. The XPS spectra show the presence of Ni, O, and C elements (Figure 6c). In Ni 2p spectra, two typical sets of broad signals corresponding to Ni $2p_{3/2}$ (856.5 eV) and Ni $2p_{1/2}$ (873.8 eV) are observed, indicating the Ni element is in a range of typical Ni^{2+} or Ni^{3+} bound to oxygen (Figure 6d).[32,48] The XPS data show that the element ratio of C, O, and Ni in the O_2-NiO_x-MWCNTs film is 18.8:6.7:1.0 (51.07%, 18.22%, and 2.72%, for C, O, and Ni, respectively), demonstrating that the O content is higher than that in the H_2-NiO_x-MWCNTs film. Similar to the previous analysis for H_2-NiO_x-MWCNTs film, the O_2-NiO_x-MWCNTs film probably contains $Ni(OH)_2$, but the presence of NiOOH is not excluded. The EDX and XPS results indicate that the elemental components of O_2-NiO_x-MWCNTs are similar to those of the H_2-NiO_x-MWCNTs for water reduction, but the oxygen content is obviously higher in the O_2-NiO_x-MWCNTs for water oxidation (Figures 2 and 6). Powder X-ray diffraction data show that the NiO_x species from both H_2-NiO_x-MWCNTs and O_2-NiO_x-MWCNTs electrodes have amorphous character with no typical diffraction peaks of nickel based materials (Figure S5, Supporting Information).

Finally, the H_2-NiO_x-MWCNTs film electrodeposited at −1.2 V was used for both OER and HER in the same electrochemical cell (Figure 7). The film was obtained after 1 C of charges passed through the electrode at −1.2 V and then transferred to a 0.1 M nickel-free KBi solution (pH 9.2). After 1 h of bulk electrolysis at +1.1 V, the potential was switched to the reductive condition (−1.2 V). The stable current density was about −1.0 mA/cm^2 at the −1.2 V for hydrogen reduction and 1.5 mA/cm^2 at +1.1 V for water oxidation. The switch between HER and OER shows good reversibility. The results demonstrate that the NiO_x-MWCNTs film is highly efficient for both OER and HER and that the film has good stability during bulk electrolysis for water splitting.

■ CONCLUSIONS

The results reported here show nickel-based thin films on MWCNTs that do not require precious metals yet are highly effective for both hydrogen reduction and water oxidation. The H_2-NiO_x-MWCNTs film was prepared by reduction-induced electrodeposition in KBi buffered solution containing Ni^{2+}, and it catalyzes water splitting effectively under nearly neutral pH value. EDX spectra and XPS data indicated that the NiO_x-MWCNT film contains Ni, O, C, and K elements in the process of both water reduction and water oxidation and that the content of O is raised during OER. The NiO_x-MWCNTs electrocatalyst can effectively catalyze water oxidation at a low overpotential, which might be attributed to the excellent conductivity of MWCNTs in transporting electrons. The NiO_x-

MWCNTs electrocatalyst also has good stability, and the water-splitting catalysis is reversible when the applied potential is switched from reduction to oxidation. The efficiency of hydrogen and oxygen production is >95% in the present systems.

■ ASSOCIATED CONTENT

Ⓢ Supporting Information

Additional characterization data; TEM images; EDX spectrum; and powder XRD data. This material is available free of charge via the Internet at http://pubs.acs.org.

■ AUTHOR INFORMATION

Corresponding Author

*E-mail: dupingwu@ustc.edu.cn.

Notes

The authors declare no competing financial interest.

■ ACKNOWLEDGMENTS

This work was financially supported by the National Natural Science Foundation of China (21271166), the Fundamental Research Funds for the Central Universities (WK2060140015 and WK2060190026), the Program for New Century Excellent Talents in University (NCET), and the Thousand Young Talents Program.

■ REFERENCES

(1) Eisenberg, R.; Gray, H. B. Preface on Making Oxygen. *Inorg. Chem.* **2008**, *47*, 1697−1699.
(2) Gray, H. B. Powering the Planet with Solar Fuel. *Nature* **2009**, *1*, 7.
(3) Lewis, N. S.; Nocera, D. G. Powering the Planet: Chemical Challenges in Solar Energy Utilization. *Proc. Natl. Acad. Sci. U.S.A.* **2006**, *103*, 15729−15735.
(4) Alstrum-Acevedo, J. H.; Brennaman, M. K.; Meyer, T. J. Chemical Approaches to Artificial Photosynthesis. 2. *Inorg. Chem.* **2005**, *44*, 6802−6827.
(5) Du, P.; Knowles, K.; Eisenberg, R. A Homogeneous System for the Photogeneration of Hydrogen from Water Based on a Platinum-(II) Terpyridyl Acetylide Chromophore and a Molecular Cobalt Catalyst. *J. Am. Chem. Soc.* **2008**, *130*, 12576−12577.
(6) Dempsey, J. L.; Brunschwig, B. S.; Winkler, J. R.; Gray, H. B. Hydrogen Evolution Catalyzed by Cobaloximes. *Acc. Chem. Res.* **2009**, *42*, 1995−2004.
(7) Dismukes, G. C.; Brimblecombe, R.; Felton, G. A. N.; Pryadun, R. S.; Sheats, J. E.; Spiccia, L.; Swiegers, G. F. Development of Bioinspired Mn_4O_4-Cubane Water Oxidation Catalysts: Lessons from Photosynthesis. *Acc. Chem. Res.* **2009**, *42*, 1935−1943.
(8) Du, P.; Eisenberg, R. Catalysts Made of Earth-Abundant Elements (Co, Ni, Fe) for Water Splitting: Recent Progress and Future Challenges. *Energy Environ. Sci.* **2012**, *5*, 6012−6021.
(9) Duan, L.; Tong, L.; Xu, Y.; Sun, L. Visible Light-Driven Water Oxidation−from Molecular Catalysts to Photoelectrochemical Cells. *Energy Environ. Sci.* **2011**, *4*, 3296−3313.
(10) Gerken, J. B.; McAlpin, J. G.; Chen, J. Y. C.; Rigsby, M. L.; Casey, W. H.; Britt, R. D.; Stahl, S. S. Electrochemical Water Oxidation with Cobalt-Based Electrocatalysts from pH 0−14: The Thermodynamic Basis for Catalyst Structure, Stability, and Activity. *J. Am. Chem. Soc.* **2011**, *133*, 14431−14442.
(11) Li, G. F.; Yu, H. M.; Song, W.; Wang, X. Y.; Li, Y. K.; Shao, Z. G.; Yi, B. L. Zeolite-Templated $Ir_xRu_{1-x}O_2$ Electrocatalysts for Oxygen Evolution Reaction in Solid Polymer Electrolyte Water Electrolyzers. *Int. J. Hydrogen Energy* **2012**, *37*, 16786−16794.
(12) Liang, Y. Y.; Li, Y. G.; Wang, H. L.; Zhou, J. G.; Wang, J.; Regier, T.; Dai, H. J. Co_3O_4 Nanocrystals on Graphene as a Synergistic Catalyst for Oxygen Reduction Reaction. *Nat. Mater.* **2011**, *10*, 780−786.
(13) McEvoy, J. P.; Brudvig, G. W. Water-Splitting Chemistry of Photosystem II. *Chem. Rev.* **2006**, *106*, 4455−4483.
(14) Nocera, D. G. The Artificial Leaf. *Acc. Chem. Res.* **2012**, *45*, 767−776.
(15) Liu, F. S.; Ji, R.; Wu, M.; Sun, Y. M. Hydrogen Production from Water Splitting Using Perylene Dye-Sensitized Pt/TiO_2 Photocatalyst. *Acta Phys.-Chim. Sin.* **2007**, *23*, 1899−1904.
(16) Smotkin, E.; Bard, A. J.; Campion, A.; Fox, M. A.; Mallouk, T.; Webber, S. E.; White, J. M. Bipolar TiO_2/Pt Semiconductor Photoelectrodes and Multielectrode Arrays for Unassisted Photolytic Water Splitting. *J. Phys. Chem.* **1986**, *90*, 4604−4607.
(17) Du, P.; Schneider, J.; Jarosz, P.; Eisenberg, R. Photocatalytic Generation of Hydrogen from Water Using a Platinum(II) Terpyridyl Acetylide Chromophore. *J. Am. Chem. Soc.* **2006**, *128*, 7726−7727.
(18) Duan, L.; Bozoglian, F.; Mandal, S.; Stewart, B.; Privalov, T.; Llobet, A.; Sun, L. A Molecular Ruthenium Catalyst with Water-Oxidation Activity Comparable to That of Photosystem II. *Nat. Chem.* **2012**, *4*, 418−423.
(19) Meyer, T. J.; Huynh, M. H. V. The Remarkable Reactivity of High Oxidation State Ruthenium and Osmium Polypyridyl Complexes. *Inorg. Chem.* **2003**, *42*, 8140−8160.
(20) Zhao, Y. X.; Hernandez-Pagan, E. A.; Vargas-Barbosa, N. M.; Dysart, J. L.; Mallouk, T. E. A High Yield Synthesis of Ligand-Free Iridium Oxide Nanoparticles with High Electrocatalytic Activity. *J. Phys. Chem. Lett.* **2011**, *2*, 402−406.
(21) Hinnemann, B.; Moses, P. G.; Bonde, J.; Jorgensen, K. P.; Nielsen, J. H.; Horch, S.; Chorkendorff, I.; Norskov, J. K. Biornimetic Hydrogen Evolution: MoS_2 Nanoparticles as Catalyst for Hydrogen Evolution. *J. Am. Chem. Soc.* **2005**, *127*, 5308−5309.
(22) Jaramillo, T. F.; Jorgensen, K. P.; Bonde, J.; Nielsen, J. H.; Horch, S.; Chorkendorff, I. Identification of Active Edge Sites for Electrochemical H_2 Evolution from MoS_2 Nanocatalysts. *Science* **2007**, *317*, 100−102.
(23) Kibsgaard, J.; Chen, Z. B.; Reinecke, B. N.; Jaramillo, T. F. Engineering the Surface Structure of MoS_2 to Preferentially Expose Active Edge Sites for Electrocatalysis. *Nat. Mater.* **2012**, *11*, 963−969.
(24) Merki, D.; Fierro, S.; Vrubel, H.; Hu, X. L. Amorphous Molybdenum Sulfide Films as Catalysts for Electrochemical Hydrogen Production in Water. *Chem. Sci.* **2011**, *2*, 1262−1267.
(25) Chen, W. F.; Sasaki, K.; Ma, C.; Frenkel, A. I.; Marinkovic, N.; Muckerman, J. T.; Zhu, Y. M.; Adzic, R. R. Hydrogen-Evolution Catalysts Based on Non-Noble Metal Nickel-Molybdenum Nitride Nanosheets. *Angew. Chem., Int. Ed.* **2012**, *51*, 6131−6135.
(26) McKone, J. R.; Sadtler, B. F.; Werlang, C. A.; Lewis, N. S.; Gray, H. B. Ni-Mo Nanopowders for Efficient Electrochemical Hydrogen Evolution. *ACS Catal.* **2013**, *3*, 166−169.
(27) Barber, J. Photosynthetic Energy Conversion: Natural and Artificial. *Chem. Soc. Rev.* **2009**, *38*, 185−196.
(28) Bricker, T. M.; Roose, J. L.; Fagerlund, R. D.; Frankel, L. K.; Eaton-Rye, J. J. The Extrinsic Proteins of Photosystem II. *Biochim. Biophys. Acta* **2012**, *1817*, 121−142.
(29) Gong, M.; Li, Y. G.; Wang, H. L.; Liang, Y. Y.; Wu, J. Z.; Zhou, J. G.; Wang, J.; Regier, T.; Wei, F.; Dai, H. J. An Advanced Ni-Fe Layered Double Hydroxide Electrocatalyst for Water Oxidation. *J. Am. Chem. Soc.* **2013**, *135*, 8452−8455.
(30) Li, F.; Zhang, B. B.; Li, X. N.; Jiang, Y.; Chen, L.; Li, Y. Q.; Sun, L. C. Highly Efficient Oxidation of Water by a Molecular Catalyst Immobilized on Carbon Nanotubes. *Angew. Chem., Int. Ed.* **2011**, *50*, 12276−12279.
(31) Liang, Y. Y.; Wang, H. L.; Diao, P.; Chang, W.; Hong, G. S.; Li, Y. G.; Gong, M.; Xie, L. M.; Zhou, J. G.; Wang, J.; Regier, T. Z.; Wei, F.; Dai, H. J. Oxygen Reduction Electrocatalyst Based on Strongly Coupled Cobalt Oxide Nanocrystals and Carbon Nanotubes. *J. Am. Chem. Soc.* **2012**, *134*, 15849−15857.
(32) Mansour, A. N.; Melendres, C. A.; Pankuch, M.; Brizzolara, R. A. X-Ray-Absorption Fine-Structure Spectra and the Oxidation-State

of Nickel in Some of Its Oxycompounds. *J. Electrochem. Soc.* **1994**, *141*, L69−L71.
(33) Reece, S. Y.; Hamel, J. A.; Sung, K.; Jarvi, T. D.; Esswein, A. J.; Pijpers, J. J. H.; Nocera, D. G. Wireless Solar Water Splitting Using Silicon-Based Semiconductors and Earth-Abundant Catalysts. *Science* **2011**, *334*, 645−648.
(34) Cobo, S.; Heidkamp, J.; Jacques, P. A.; Fize, J.; Fourmond, V.; Guetaz, L.; Jousselme, B.; Ivanova, V.; Dau, H.; Palacin, S.; Fontecave, M.; Artero, V. A Janus Cobalt-based Catalytic Material for Electro-splitting of Water. *Nat. Mater.* **2012**, *11*, 802−807.
(35) He, C. Y.; Wu, X. L.; He, Z. Q. Amorphous Nickel-Based Thin Film as a Janus Electrocatalyst for Water Splitting. *J. Phys. Chem. C* **2014**, *118*, 4578−4584.
(36) Lim, S. C.; Choi, L. C.; Jeong, H. J.; Shin, Y. M.; An, K. H.; Bae, D. J.; Lee, Y. H.; Lee, N. S.; Kim, J. M. Effect of Gas Exposure on Field Emission Properties of Carbon Nanotube Arrays. *Adv. Mater.* **2001**, *13*, 1563−1567.
(37) Lota, G.; Fic, K.; Frackowiak, E. Carbon Nanotubes and Their Composites in Electrochemical Applications. *Energy Environ. Sci.* **2011**, *4*, 1592−1605.
(38) Toma, F. M.; Sartorel, A.; Iurlo, M.; Carraro, M.; Parisse, P.; Maccato, C.; Rapino, S.; Gonzalez, B. R.; Amenitsch, H.; Da Ros, T.; Casalis, L.; Goldoni, A.; Marcaccio, M.; Scorrano, G.; Scoles, G.; Paolucci, F.; Prato, M.; Bonchio, M. Efficient Water Oxidation at Carbon Nanotube-Polyoxometalate Electrocatalytic Interfaces. *Nat. Chem.* **2010**, *2*, 826−831.
(39) Chigane, M.; Ishikawa, M. XRD and XPS Characterization of Electrochromic Nickel Oxide Thin Films Prepared by Electrolysis Chemical Deposition. *J. Chem. Soc., Faraday Trans.* **1998**, *94*, 3665−3670.
(40) Mclntyre, N. S.; Cook, M. G. X-Ray Photoelectron Studies on Some Oxides and Hydroxides of Cobalt, Nickel, and Copper. *Anal. Chem.* **1975**, *47*, 2208−2213.
(41) Chigane, M.; Ishikawa, M. Characterization of Electrochromic Nickel Oxide Thin Films Prepared by Anodic Deposition. *J. Chem. Soc., Faraday Trans.* **1992**, *88*, 2203−2205.
(42) Moroney, L. M.; Smart, R. S. C.; Roberts, M. W. Studies of the Thermal Decomposition of β-NiO(OH) and Nickel Peroxide by X-ray Photoelectron Spectroscopy. *J. Chem. Soc., Faraday Trans. 1* **1983**, *79*, 1769−1778.
(43) Abd El Aal, E. E. Anodic Oxide Films on Nickel Electrode in Borate Solutions. *Corros. Sci.* **2003**, *45*, 641−658.
(44) Dinca, M.; Surendranath, Y.; Nocera, D. G. Nickel-Borate Oxygen-Evolving Catalyst that Functions under Benign Conditions. *Proc. Natl. Acad. Sci. U.S.A.* **2010**, *107*, 10337−10341.
(45) Wolf, J. F.; Yeh, L. S. R.; Damjanovic, A. Anodic Oxide-Films at Nickel Electrodes in Alkaline-Solutions 0.2. pH-Dependence and Rate Determining Step. *Electrochim. Acta* **1981**, *26*, 811−817.
(46) Dechialvo, M. R. G.; Chialvo, A. C. Oxygen Evolution Reaction on Thick Hydrous Nickel-Oxide Electrodes. *Electrochim. Acta* **1988**, *33*, 825−830.
(47) Wang, X. Y.; Luo, H.; Yang, H. P.; Sebastian, P. J.; Gamboa, S. A. Oxygen Catalytic Evolution Reaction on Nickel Hydroxide Electrode Modified by Electroless Cobalt Coating. *Int. J. Hydrogen Energy* **2004**, *29*, 967−972.
(48) Yu, X.; Xu, P.; Hua, T.; Han, A.; Liu, X.; Wu, H.; Du, P. Multi-walled Carbon Nanotubes Supported Porous Nickel Oxide as Noble Metal-Free Electrocatalysts for Efficient Water Oxidation. *Int. J. Hydrogen Energy* **2014**, *39*, 10467−10475.